Géographie physique et Quaternaire

Modeling the Cordilleran Ice Sheet
Modélisation de l'Inlandsis de la Cordillère
Modellierung der Kordilleren-Eisdecke.

Barry L. Robert

Volume 45, numéro 3, 1991

L'Inlandis de la Cordillère
The Cordilleran Ice Sheet

URI : https://id.erudit.org/iderudit/032876ar
DOI : https://doi.org/10.7202/032876ar

Aller au sommaire du numéro

Éditeur(s)

Les Presses de l'Université de Montréal

ISSN

0705-7199 (imprimé)
1492-143X (numérique)

Découvrir la revue

Citer cet article

Robert, B. L. (1991). Modeling the Cordilleran Ice Sheet. *Géographie physique et Quaternaire*, *45*(3), 287–299. https://doi.org/10.7202/032876ar

Résumé de l'article

On a élaboré un modèle d'écoulement glaciaire spatio-temporel qui permette la reconstitution précise de la croissance et du retrait de la partie centrale de l'Inlandsis de la Cordillère, au Wisconsinien supérieur. Le modèle bi-dimensionnel et temporel illustre les différentes altitudes de la surface glaciaire et les directions d'écoulement dans une grille dont les carreaux ont 15 km de côté. Les données de base comprennent la topographie sous-glaciaire, la fonction du bilan de masse net et deux paramètres de l'écoulement glaciaire. Une équation polynomiale sert a estimer l'altitude de la ligne d'équilibre dans la région à l'étude à partir de la fonction du bilan de masse net. Une équation quadratique permet ensuite d'obtenir les valeurs du bilan de masse net en tant que fonction de l'altitude relative de la ligne d'équilibre. Les conditions glaciaires au Wisconsinien supérieur sont simulées en abaissant de façon systématique l'altitude de la ligne d'équilibre. La chronologie générale de la croissance et du retrait établie dans le modèle est vérifiée par les sites datés au radiocarbone qui donnent des repères quant à l'étendue de l'inlandsis à différentes périodes de la glaciation du Wisconsinien supérieur. Les données de géologie glaciaire directement attribuables au dernier inlandsis ont également servi à vérifier le modèle. Les résultats tirés de ces expériences indiquent qu'une chronologie de la glaciation conforme aux datations au radiocarbone peut être établie en utilisant le modèle, qui livre aussi des renseignements sur les directions d'écoulement, ainsi que sur les modes de croissance et de retrait.

Géographie physique et Quaternaire, 1991, vol. 45, n° 3, p. 287-299, 17 fig.

MODELING THE CORDILLERAN ICE SHEET

Barry L. ROBERTS, EG & G Rocky Flats, Inc., Building T130B, P.O. Box 464, Golden, Colorado 80402-0464, U.S.A.

ABSTRACT A time-dependent ice flow model is used to provide detailed reconstructions of ice growth and retreat for the southern portion of the Late Wisconsinan Cordilleran Ice Sheet. The two-dimensional, time-dependent model provides ice surface elevations and flow directions at a grid spacing of 15 km. Input to the model includes subglacial topography, a net mass balance function, and two ice flow parameters. The net mass balance function uses a polynomial equation to estimate equilibrium line altitude (ELA) across the study area. A quadratic equation is then used to provide net mass balance values as a function of elevation relative to the ELA. Late Wisconsinan glacial conditions are simulated by systematically lowering the ELA. The general timing of the model ice advance and retreat is tested against radiocarbon dated localities which place limits on the ice sheet's areal extent for different times during the Late Wisconsinan glaciation. In addition, glacial-geologic evidence directly attributable to the latest Cordilleran Ice Sheet is used in assessing the model reconstructions. Results from these experiments show that an ice growth and retreat chronology consistent with the limiting radiocarbon dates can be generated using the model, and provide information on flow directions and ice growth and retreat patterns.

RÉSUMÉ *Modélisation de l'Inlandsis de la Cordillère*. On a élaboré un modèle d'écoulement glaciaire spatio-temporel qui permette la reconstitution précise de la croissance et du retrait de la partie centrale de l'Inlandsis de la Cordillère, au Wisconsinien supérieur. Le modèle bi-dimensionnel et temporel illustre les différentes altitudes de la surface glaciaire et les directions d'écoulement dans une grille dont les carreaux ont 15 km de côté. Les données de base comprennent la topographie sous-glaciaire, la fonction du bilan de masse net et deux paramètres de l'écoulement glaciaire. Une équation polynomiale sert a estimer l'altitude de la ligne d'équilibre dans la région à l'étude à partir de la fonction du bilan de masse net. Une équation quadratique permet ensuite d'obtenir les valeurs du bilan de masse net en tant que fonction de l'altitude relative de la ligne d'équilibre. Les conditions glaciaires au Wisconsinien supérieur sont simulées en abaissant de façon systématique l'altitude de la ligne d'équilibre. La chronologie générale de la croissance et du retrait établie dans le modèle est vérifiée par les sites datés au radiocarbone qui donnent des repères quant à l'étendue de l'inlandsis à différentes périodes de la glaciation du Wisconsinien supérieur. Les données de géologie glaciaire directement attribuables au dernier inlandsis ont également servi à vérifier le modèle. Les résultats tirés de ces expériences indiquent qu'une chronologie de la glaciation conforme aux datations au radiocarbone peut être établie en utilisant le modèle, qui livre aussi des renseignements sur les directions d'écoulement, ainsi que sur les modes de croissance et de retrait.

ZUSAMMENFASSUNG *Modellierung der Kordilleren-Eisdecke*. Um Eisausdehnung und Eisrückzug für den südlichen Teil der Kordilleren-Eisdecke im Spät-Wisconsin detailliert zu rekonstruieren, hat man ein zeitabhängiges Eisflußmodell benutzt. Das zweidimensionale, zeitabhängige Modell gibt Auskunft über die verschiedenen Höhen der Eisoberfläche und die Richtungen des Fließens in einem Raster von Quadraten mit 15 km Seitenlänge. Zu den Eingaben in das Modell gehören die subglaziale Topographie, die Funktion der Netto-Masse-Bilanz und zwei Eisfluß-Parameter. Die Funktion der Netto-Masse-Bilanz benutzt eine polynomische Gleichung, um die Höhe der Gleichgewichtslinie quer durch das untersuchte Gebiet abzuschätzen. Eine quadratische Gleichung wird dann benutzt, um die Werte der Netto-Masse-Bilanz als eine Funktion der Höhe in Bezug auf die Gleichgewichtslinie zu berechnen. Man simuliert die glazialen Bedingungen im späten Wisconsin, indem man die Gleichgewichtslinie systematisch senkt. Die allgemeine Chronologie des Eisvor-und Rückstoßes im Modell wird überprüft mittels Vergleich mit Plätzen, zu denen es Radiokarbondaten gibt und die der Ausdehnung der Eisfläche zu verschiedenen Zeiten während der spätwisconsinischen Vereisung Grenzen setzen. Zusätzlich werden bei der Festsetzung der Modell-Rekonstruktionen glazial-geologische Zeugnisse genutzt, die der spätesten Kordilleren-Eisdecke direkt zuzuschreiben sind. Ergebnisse dieser Experimente zeigen, daß mittels des Modells eine Eisausdehnungs- und Eisrückzugschronologie geschaffen werden kann, die mit den Grenzwerten der Radiokarbondaten übereinstimmt und Informationen über Fließrichtungen und Eisausdehnungs und Eisrückzugsmuster liefert.

Manuscrit reçu le 26 mars 1991; manuscrit révisé accepté le 20 septembre 1991

INTRODUCTION

Information about the last Cordilleran Ice Sheet comes primarily from glacial-geologic evidence left during the retreat of the ice sheet. Because much of this evidence lacks chronologic control, and because several ice flow directions may be represented at a given locality (Clague, 1975), time-dependent reconstructions of ice flow patterns cannot be made from the geologic record alone. In addition, because retreating ice can destroy or disrupt previously developed flow indicators, little is known about the pattern of ice growth and flow during buildup of the ice sheet. One method of adressing these problems is the use of ice flow modeling experiments. Ice flow modeling can assist in understanding the growth and retreat of past ice sheets by providing chronologic reconstructions of ice thickness and flow directions for the entire history of the ice sheet.

Although model-based reconstructions of the Cordilleran Ice Sheet have been presented in previous studies (*e.g.* Hughes, 1987; Denton and Hughes, 1981; Budd and Smith, 1981, 1987), these were generally included as part of comprehensive reconstructions of the North American ice sheets and as such, did not include detailed information about the Cordilleran Ice Sheet. To understand the nature of ice advance and retreat for the Cordilleran Ice Sheet requires a more concentrated modeling effort. The multiple ice source regions (Clague, 1981) and complex bedrock topogaphy of the Canadian Cordillera generate compound, time-dependent ice flow patterns. To see the development and change in these patterns requires time-dependent modeling at an appropriate scale.

This paper presents the results from time-dependent modeling of the southern portion of the Late Wisconsinan Cordilleran Ice Sheet. The simulation results address the problems discussed above by providing a detailed reconstruction of ice growth and retreat including ice thickness and flow direction information. These reconstructions were developed using a computer ice sheet model incorporating the ice flow equations presented by Mahaffy (1976). The model (Roberts, 1990) uses bedrock topography and estimated net mass balance rates to simulate the nucleation, growth, and retreat of the ice sheet.

STUDY AREA

The ice sheet reconstructions presented here concentrate on the southern portion of the Cordilleran Ice Sheet (Fig. 1). The study area covers approximately 691,000 square kilometers with solution points spaced at 15 km intervals. The grid consists of 48 rows (north-south) and 64 columns (east-west).

The boundaries of the study area were chosen so major ice source regions, such as the Coast and Rocky Mountains, were included (Fig. 2). The divide between north and south flowing Late Wisconsinan ice on the Interior Plateau of British Columbia (Prest *et al.*, 1968) was used to define the northern boundary of the area. The southern boundary was set to include all the lobes of the maximum Late Wisconsinan advance.

PROCEDURE

The model constructed for this study computes ice surface elevations and flow velocities for a series of equally spaced grid

FIGURE 1. Location of study area relative to entire Cordilleran Ice Sheet. Stippled pattern shows regions that were covered by ice during the Late Wisconsinan (ice extent from Clague, 1989).

Localisation de la région à l'étude par rapport à l'ensemble de l'Inlandsis de la Cordillère. La trame montre la région recouverte de glace au cours du Wisconsinien supérieur (d'après Clague, 1989).

points covering a rectangular region. The main input requirements are the land surface elevation (Fig. 3), and the net mass balance for each grid point in the study area. An empirical function is used to specify net mass balance values. Changes in equilibrium line altitude specified using a time-dependent ELA history curve drive ice sheet growth and decay.

The model steps through time, computing net mass balance, ice flow, and resulting ice surface elevation for every grid point at each timestep. Points with a positive mass balance accumulate ice which, after attaining sufficient thickness, begins to flow. The model does not restrict accumulation areas. Isolated alpine glaciers and ice caps unrelated to the Cordilleran Ice Sheet can develop during the simulation.

Important assumptions and simplifications made during formulation of the model include: 1) the ice is isothermal; 2) basal sliding of the ice is not explicitly modeled; 3) the subglacial bed does not deform; 4) no mechanism for ablation through calving is included; 5) isostatic compensation is not included.

These assumptions were made in order to simplify the numerical solutions or because the represented process could not be adequately parameterized for the Late Wisconsinan Cordilleran Ice Sheet.

ICE FLOW EQUATIONS

Ice flow computations are made using the two-dimensional ice flow equations presented by Mahaffy (1976). These equa-

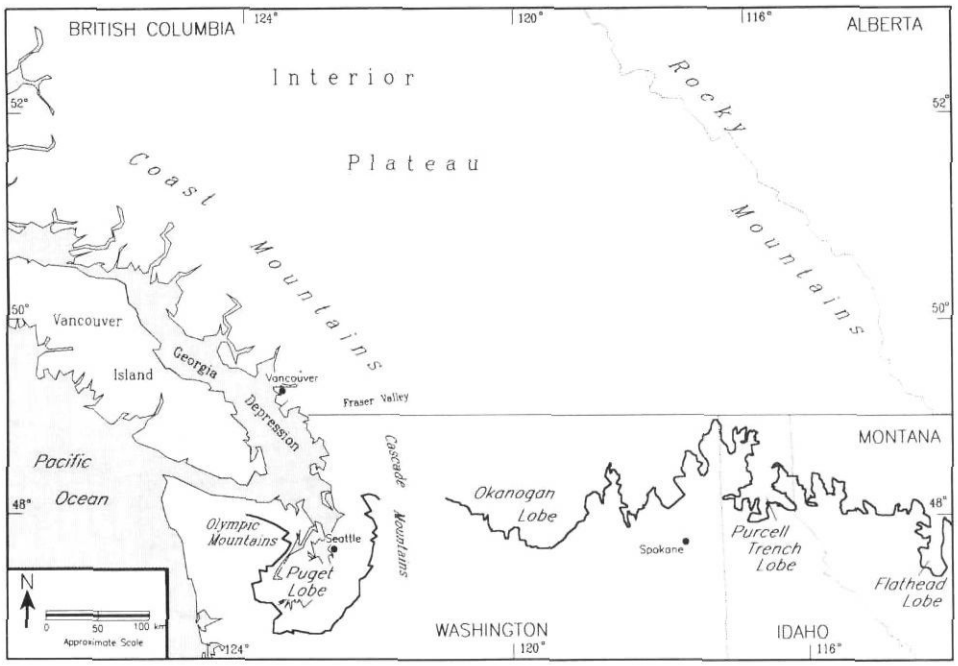

FIGURE 2. Major physiographic and cultural features of the study area. Heavy line shows the maximum southern margin of the Late Wisconsinan Cordilleran Ice Sheet with the major ice lobes labeled.

Principales entités physiographiques de la région à l'étude. Le trait gras illustre la limite méridionale de l'Inlandsis de la Cordillère au Wisconsinien supérieur.

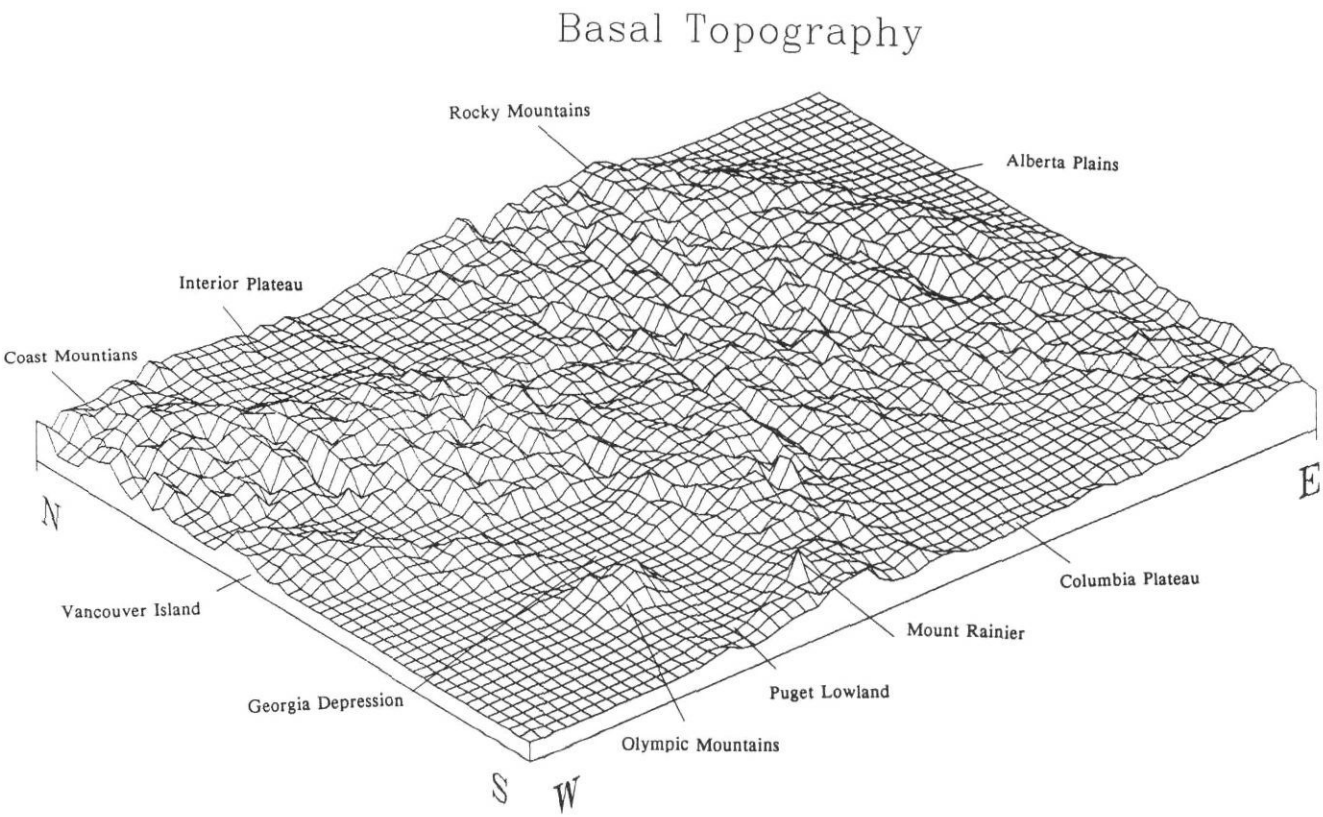

FIGURE 3. Oblique view of study area showing digital terrain data used in the model. Major topographic features are noted. Spacing between grid lines is 15 km and vertical exaggeration is 50.

Modèle de la topographie de la région étudiée en vue oblique. Les carreaux ont 15 km de côté et l'exagération verticale est de 50.

tions provide ice height values for a two-dimensional plan-view grid. In this grid, the x and y axes are perpendicular to each other and lie in a surface parallel to the geoid. Ice flow is computed in the x and y directions for each grid point in the solution area.

The fundamental relationship for determining the change in ice height with time is a two-dimensional continuity of mass equation.

$$(1) \qquad \frac{\delta h}{\delta t} = a(x,y,t) - \left\{ \frac{\delta q_x}{\delta x} + \frac{\delta q_y}{\delta y} \right\}$$

In the above equation h represents the elevation of the ice surface, t is time, a is the mass gain or loss by accumulation or ablation, and q_x and q_y represent the mass flux in the x and y directions respectively.

Accumulation and ablation are specified in the model using a net mass balance function. The mass flux terms are calculated using the ice surface slope and thickness.

$$(2) \qquad q_x = \left\{ \frac{-2A^{-n}}{n+2} \right\} (\rho g)^n \frac{\delta h}{\delta x} \alpha^{(n-1)} (h\text{-}z_0)^{n+2}$$

$$(3) \qquad q_y = \left\{ \frac{-2A^{-n}}{n+2} \right\} (\rho g)^n \frac{\delta h}{\delta y} \alpha^{(n-1)} (h\text{-}z_0)^{n+2}$$

where:

A and n are flow law parameters dependent on various ice properties, ρ is the ice density, g is gravitational acceleration, z_o is the subglacial landform elevation, and α is the ice surface slope in the direction of flow defined as

$$(4) \qquad \alpha = \left(\left[\frac{\delta h}{\delta x} \right]^2 + \left[\frac{\delta h}{\delta y} \right]^2 \right)^{1/2}$$

The ice flow equations are implemented as finite difference equations using an Alternating Direction Implicit formulation such as used by Mahaffy (1976). The flow law exponent, n, was set equal to two for the results shown here based on initial simulations. The flow law coefficient, A, was chosen for ice between 0°C and −5°C based on values presented in Mahaffy (1974).

Assumptions made during the formulation of the above ice flow equations as defined by Mahaffy (1976) are: 1) the ice deforms only by shear strain in the xy plane; 2) the rate of horizontal change in shear stress in the ice are much less than the rate of pressure change with depth; 3) the rate of change in vertical ice velocities in the x and y directions are much smaller than the rate of change in horizontal velocities with depth. Further discussion of these assumptions can be found in Mahaffy (1976) and Roberts (1990).

NET MASS BALANCE VALUES

Net mass balance values, as a function of equilibrium line altitude (ELA), control the gain or loss of ice mass at each grid point within the simulation domain. Net mass balance values are determined using a two step procedure. First, the ELA for the given location is determined. Second, the vertical distance between the equilibrium line and the present surface elevation is computed. This vertical distance is then used to calculate the net mass balance from a function relating elevation relative to the ELA to net mass balance.

Modern ELA in the model is represented by a trend surface equation which estimates ELA (in meters) as a function of latitude (Θ) and longitude (Φ) in decimal degrees. The elevation of each point on the plane described by this equation, listed as equation (5) below, represents the modern regional ELA for that geographic location. This plane can be shifted vertically to simulate different climatic conditions. For example, a 600 m decrease in ELA would be represented by lowering the plane 600 m.

$$(5) \qquad ELA(m) = 14306.8 + (-70.44\,\Phi) + (-70.35\,\Theta)$$

This trend surface equation was developed using an all possible subsets regression procedure and ELA data from 18 glaciers in western North America (Haeberli and Muller, 1988; Haeberli, 1985; Meier *et al.*, 1971) and explains 82% of the variance in the observations.

The ELA function is intended to represent the regional changes in ELA associated with variations in continentality and latitude; no attempt has been made to replicate the topographically-controlled second-order details of the modern equilibrium altitude surface such as described by Porter (1977).

Net mass balance is computed as a function of elevation relative to the ELA derived using data from 11 modern glaciers in British Columbia and Alberta (Haeberli and Muller 1988). Following the method of Porter *et al.* (1983) and Booth (1986), net mass balance information from the individual glaciers were adjusted to a common elevation axis based on vertical distance relative to the ELA. The equilibrium line of each curve was set to an elevation of zero; positive and negative elevations yield positive and negative net mass balance values respectively. An all possible subsets second-order polynomial regression was performed on the data to obtain the quadratic equation which was used to provide net mass balance values (Fig. 4).

Because the modern glaciers used to develop the mass balance curve in Figure 4 are relatively small, some adjustments were made to the positive value rates so that they would be more appropriate for a large ice sheet such as the Cordilleran.

Because the accumulation rate over large ice sheets is known to be relatively low (Radok *et al.*, 1982) a limit of one m/yr was placed on the maximum positive net mass balance rate derived from the net mass balance curve (Hughes, 1985, fig. 1; Oerlemans, 1981; Andrews and Mahaffy, 1976). A limit of −15 m/yr was placed on the maximum negative net mass balance rate so these values would remain within reasonable bounds (Budd and Smith, 1981).

An "elevation-desert effect" was also incorporated into the model. This is intended to reproduce the decrease in positive net mass balance rate with increasing altitude often seen over large ice sheets (Budd and Smith, 1981). The elevation-desert effect model used here is similar to that used by Budd and Smith (1981). In it, net mass balance (a) is reduced as a function of elevation (ε), in kilometers, above a defined threshold (τ), to obtain the reduced net mass balance value (a'), as shown below.

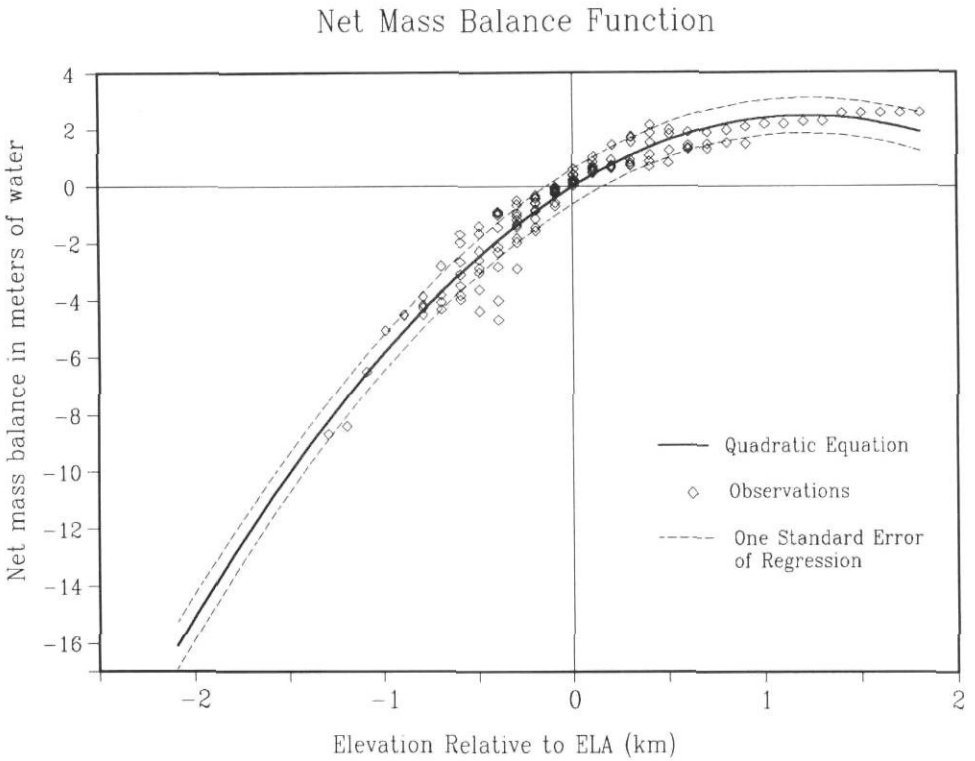

FIGURE 4. Observational data and resulting net mass balance curve used to provide net mass balance values.

Les données d'observation et la courbe de bilan de masse net sur lesquelles on s'est fondé pour obtenir les valeurs du bilan de masse net.

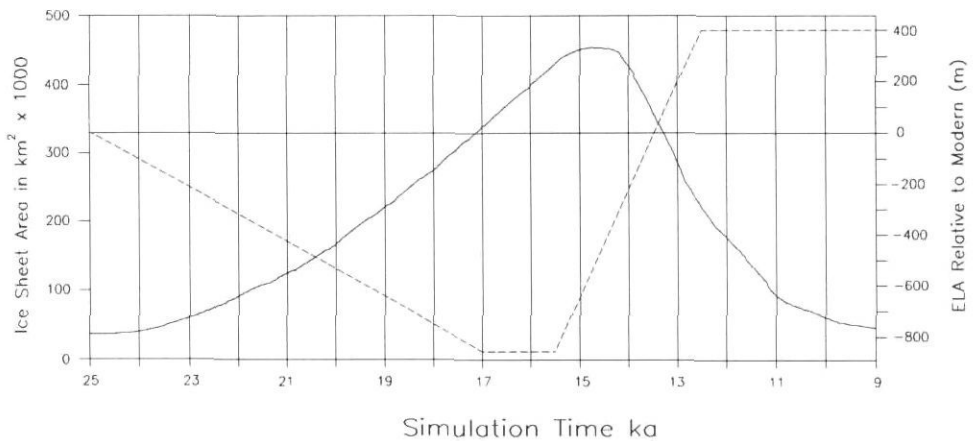

FIGURE 5. ELA history curve (dashed line) and resulting ice sheet area (solid line) from Late Wisconsinan simulation.

Courbe de l'évolution de l'altitude de la ligne d'équilibre (tirets) et superficie de l'inlandsis découlant de la simulation de l'évolution glaciaire du Wisconsinien supérieur.

(6) $$a' = a / 2^{(\varepsilon - \tau)}$$

This function is only applied to points where there is ice present, there is a positive net mass balance, and the ice surface elevation is above the threshold (τ) of two kilometers.

LATE WISCONSINAN SIMULATION

This section discusses the procedures used in reconstructing the growth and retreat history of the Late Wisconsinan Cordilleran Ice Sheet and presents the results from this modeling.

Reconstruction of a realistic growth and retreat chronology for the Late Wisconsinan Cordilleran Ice Sheet relies on providing the necessary driving function for ice growth and retreat. In the model, this driving function is represented by a curve representing time-dependent changes in ELA. An initial estimate of the shape of this curve was made using information available from the geologic record. This initial curve was then modified, in a plausible manner, based on the ice growth and retreat chronology generated by the model to obtain an ice growth and retreat chronology more consistent with the geologic evidence.

Parametrization of the initial ELA history curve was based on estimates of the magnitude of ELA depression (Porter *et al.*, 1983), general timing of the ice sheet growth and decay (Clague, 1981; Fulton, 1984), and paleoclimatic considerations (Heusser *et al.*, 1980; COHMAP, 1988). The maximum ELA depression (850 m) (Fig. 5) represents a typical value for alpine glaciers in the Cascade Mountains for the time period between

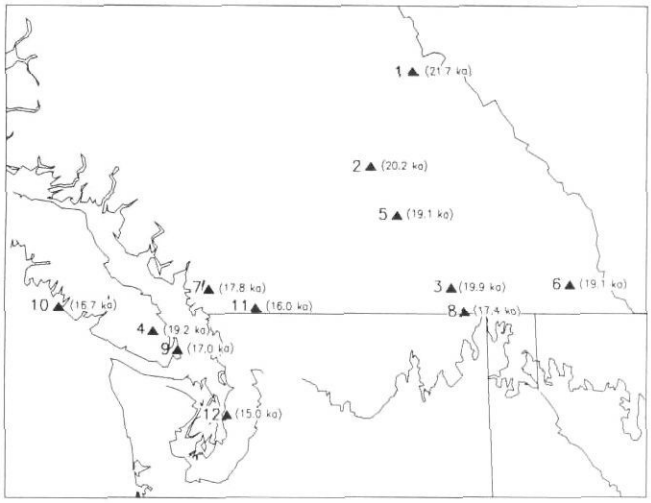

Location	Age (ka)	Source
1	21.7 ± .24	Clague, 1980
2	20.2 ± .27	Clague, 1980
3	19.9 ± .23	Clague, 1980
4	19.2 ± .25	Clague, 1980
5	19.1 ± .24	Clague, 1980
6	19.1 ± .85	Clague, 1980
7	17.8 ± .15	Clague, 1980
8	17.4 ± .33	Clague, 1980
9	17.0 ± .24	Clague, 1980
10	16.7 ± .15	Clague, 1980
11	16.0 ± .15	Clague *et al.*, 1980
12	15.0 ± .40	Mullineaux *et al.*, 1965

FIGURE 6. Ice limiting radiocarbon date localities for ice advance. Location is shown by solid triangle. Location number, to left of triangle, is keyed to accompanying table. Maximum Late Wisconsinan ice margin is also shown.

Sites des datations au radiocarbone repères de l'avancée glaciaire. Les triangles identifient les emplacements. Les chiffres, à gauche du triangle, correspondent à ceux du tableau. On indique également la limite glaciaire maximale.

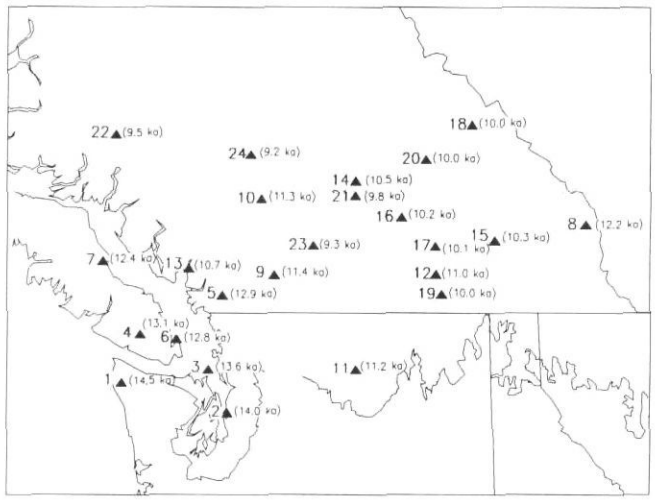

Location	Age (ka)	Source
1	14.5 ± .20	Heusser, 1973
2	14.0 ± .90	Easterbrook, 1986
3	13.6 ± .35	Booth, 1987
4	13.1 ± .13	Clague, 1980
5	12.9 ± .17	Clague, 1980
6	12.8 ± .17	Clague, 1980
7	12.4 ± .14	Clague, 1980
8	12.2 ± .16	Clague, 1980
9	11.4 ± .15	Clague, 1980
10	11.3 ± .10	Clague, 1980
11	11.2	Porter, 1978 Mehringher *et al.*, 1984
12	11.0 ± .18	Clague, 1980
13	10.7 ± .18	Clague, 1980
14	10.5 ± .17	Clague, 1980
15	10.3 ± .19	Clague, 1980
16	10.2 ± .19	Clague, 1980
17	10.1 ± .15	Clague, 1980
18	10.0 ± .14	Clague, 1980
19	10.0 ± .15	Clague, 1980
20	10.0 ± .15	Clague, 1980
21	9.8 ± .17	Clague, 1980
22	9.5 ± .16	Clague, 1980
23	9.3 ± .16	Clague, 1980
24	9.2 ± .15	Clague, 1980

FIGURE 7. Ice limiting radiocarbon date localities for ice retreat. Location is shown by solid triangle. Location number, to left of triangle, is keyed to accompanying table. Maximum Late Wisconsinan ice margin is also shown.

Sites des datations au radiocarbone repères du retrait glaciaire. Les triangles identifient les emplacements. Les chiffres, à gauche du triangle, correspondent à ceux du tableau. On indique également la limite glaciaire maximale.

approximately 25 and 15 ka (Porter *et al.*, 1983, fig. 4.12). Although there were several fluctuations of ELA in this region during this time period (Porter *et al.*, 1983), this level of detail is not considered in the model.

The results presented here show simulation results from an ELA history curve which was modified from the initial assumed curve. These modifications were implemented based on the results from initial simulations in which the general ice advance and retreat chronology was tested using radiocarbon dated ice-free locations as discussed below.

In the final modified ELA history curve (Fig. 5) the decline of the ELA starts at 25 ka, the latest time that cooling related to the buildup of the last Cordilleran Ice Sheet is believed to have started (Fulton, 1984). This timing is also consistent with paleoclimatic reconstructions for the Olympic Peninsula (Heusser *et al.*, 1980). The ELA is steadily decreased from modern levels to the maximum depression, then remains constant for some time, after which it rises quickly. The final ELA, 400 m above modern, is maintained for the remainder of the simulation to produce the rapid disintegration of the ice sheet recorded in the geologic record (Clague, 1981). Initial simulations with the final ELA at modern level did not allow rapid ice sheet disintegration (Roberts, 1990). An ELA above modern during deglaciation is also consistent with summertime insolation higher than modern at this time (COHMAP, 1988).

Radiocarbon dates which limit the areal extent of the last Cordilleran Ice Sheet (Figs. 6 and 7) are used to test the gen-

eral timing of the model's ice advance and retreat. These dates represent times when the locality was free of ice. For ice advance limiting dates, the location is considered to be ice free until at least that time; for retreat limiting dates, the location is considered to be ice free by at least that time. If a radiocarbon dated locality is within the model's ice sheet margin then this indicates the model's ice extent is expanding too quickly or retreating too slowly. The dates listed were selected from the available data to place the closest limits on the maximum extent of the ice sheet.

DISCUSSION OF RESULTS

Figure 5 shows total ice area versus time for the entire length of the simulation. The simulation starts with an initial ice configuration as computed using a modern ELA level. This follows evidence suggesting that climatic conditions in the study area prior to the main growth of the last Cordilleran Ice Sheet were similar to present (Alley, 1979; Heusser *et al.*, 1980; Clague, 1981). As the ELA drops, the area covered with ice increases steadily. The ice sheet reaches its maximum areal extent between 15 and 14 ka which agrees well with the suggested timing of the Late Wisconsinan Cordilleran Ice Sheet maximum (Clague, 1981; Easterbrook, 1986). The areal extent of the ice sheet begins to decrease approximately 1000 years after the ELA has started to rise. Deglaciation occurs rapidly from 14 to 11 ka at which point the rate of ice loss drops substantially.

Figure 8 shows the ice configuration at the start of the simulation. This configuration was generated by running the model for 5000 years with the ELA set at modern levels. For comparison the actual modern ice extent is also shown. Differences between these two ice configurations can be attributed to two major factors: topographic smoothing from the digital elevation data used as basal topography, and uncertainty in the trend surface equation (equation 5) used in estimating the ELA surface (Roberts, 1990).

Figures 9 through 16 show the results from the simulation at 2000 year time increments. The upper diagram shows ice surface elevations. Dashed lines represent ice elevation contours starting at 1500 m and increasing in 500 m increments. The thicker, outermost line represents the ice margin. Solid triangles indicate radiocarbon dated localities which should be ice free at this stage of the simulation. The lower diagram shows ice flow velocities computed by the model. The length of the ice flow vector is proportional to the magnitude of the velocity. The maximum Late Wisconsinan southern ice margin is also shown. Observations concerning these results are given below.

23 ka

After 2000 simulated years of ice growth, major ice covered areas in the Coast and Rocky Mountains have formed by expansion of glaciers present at the start of the simulation (Fig. 9). Isolated alpine glaciers appear scattered throughout the study area. All the radiocarbon dated localities lie exterior to the ice indicating that this stage of the simulation is consistent with the available geologic evidence.

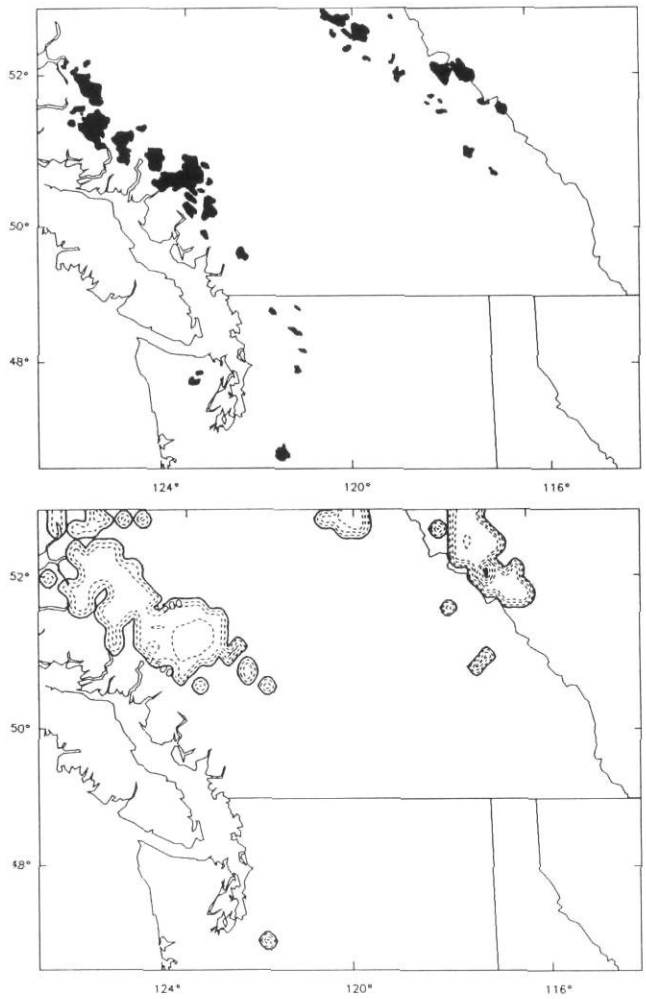

FIGURE 8. Modern ice configuration in the study area (top) and model results after a 5000 year simulation with ELA set to modern level (bottom).

Configuration moderne des glaces dans la région à l'étude (haut) et modèle qui résulte d'une simulation sur 5000 ans fondée sur le niveau actuel de la ligne d'équilibre (bas).

21 ka

The Coast Mountain ice mass is expanding more rapidly than the Rocky Mountain ice (Fig. 10). East-flowing ice from the east flank of the Coast Mountains shows the highest rate of ice front advance. Although an integrated flow system has not yet developed, ice in the Rocky Mountain region has advanced slightly. All radiocarbon date locations lie outside of the ice margin.

19 ka

The Coast and Rocky Mountain ice masses have joined into one continuous ice sheet (Fig. 11). Ice sheet elevations above 3000 m are now present in the Rocky Mountain area. East flowing ice from the Coast Mountains is being deflected southward as it meets ice from the Rocky Mountains. Fjords along the west flank of the Coast Mountains contain ice streams flowing into the Georgia Depression. A significant independent ice mass has developed in the central portion of the study area along the 49th parallel.

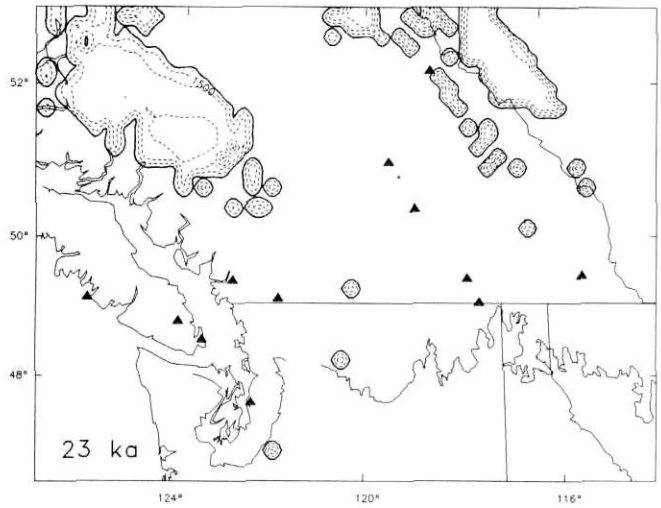

FIGURE 9. Ice configuration at 23 ka.

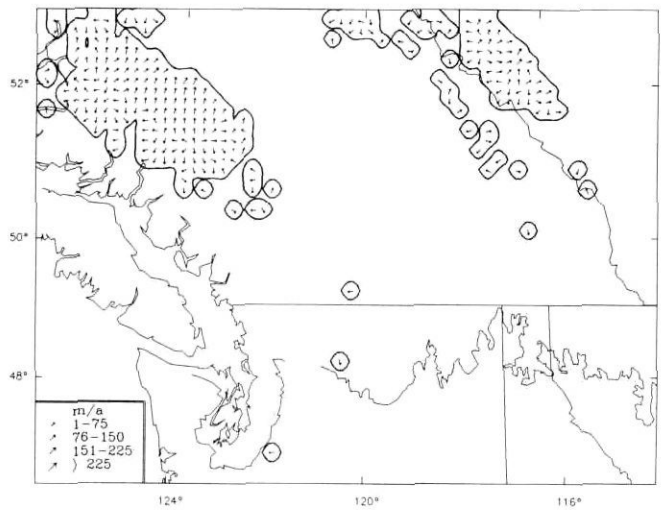

Configuration des glaces à 23 ka.

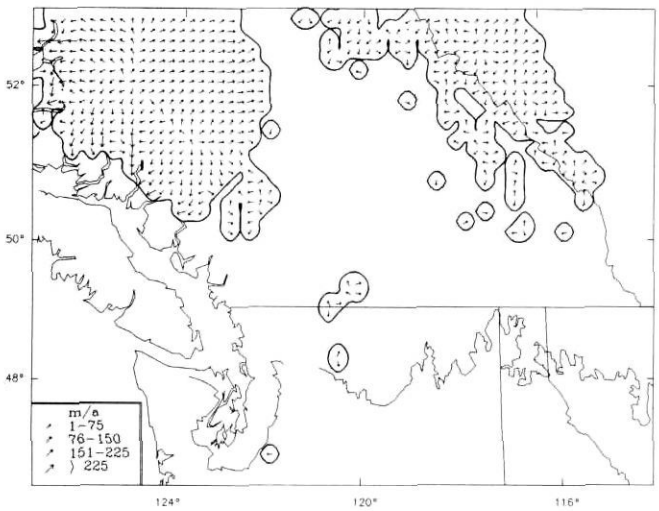

FIGURE 10. Ice configuration at 21 ka.

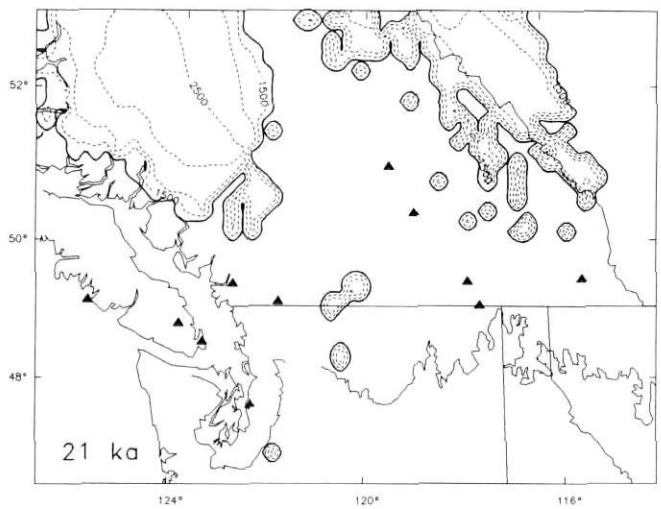

Configuration des glaces à 21 ka.

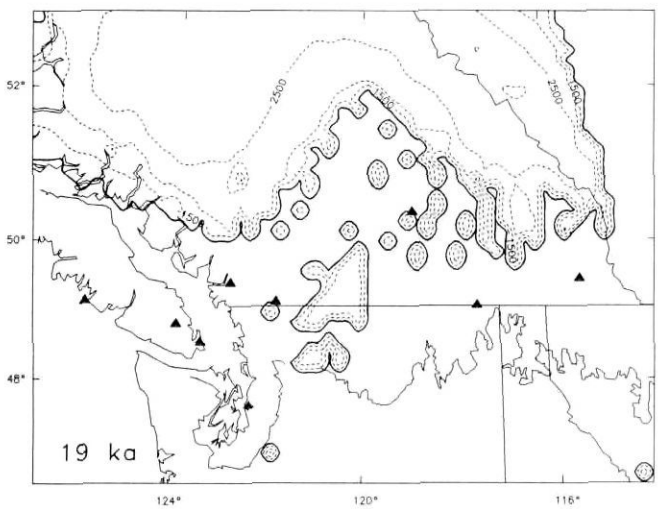

FIGURE 11. Ice configuration at 19 ka.

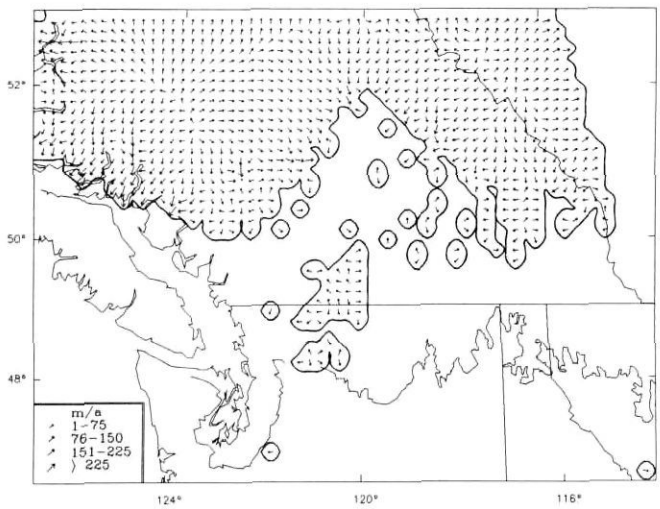

Configuration des glaces à 19 ka.

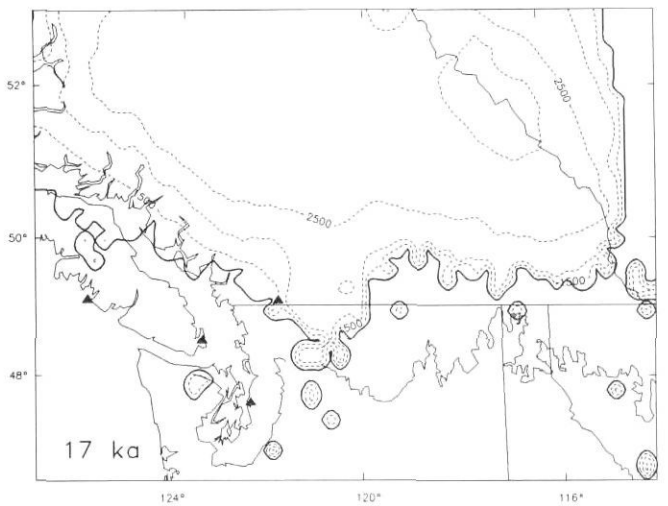

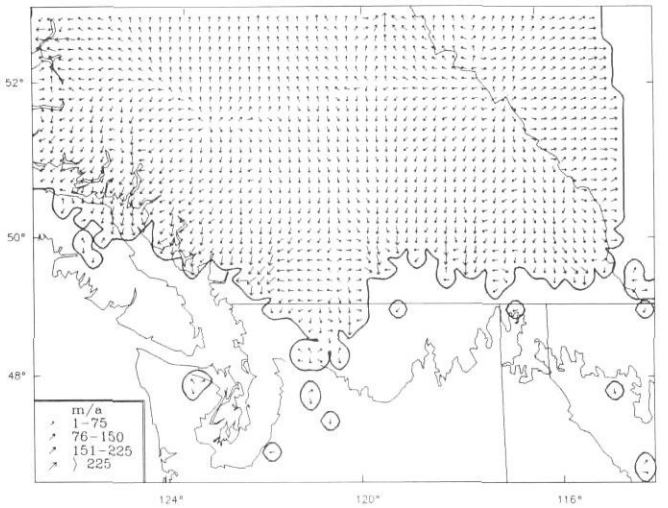

FIGURE 12. Ice configuration at 17 ka.

Configuration des glaces à 17 ka.

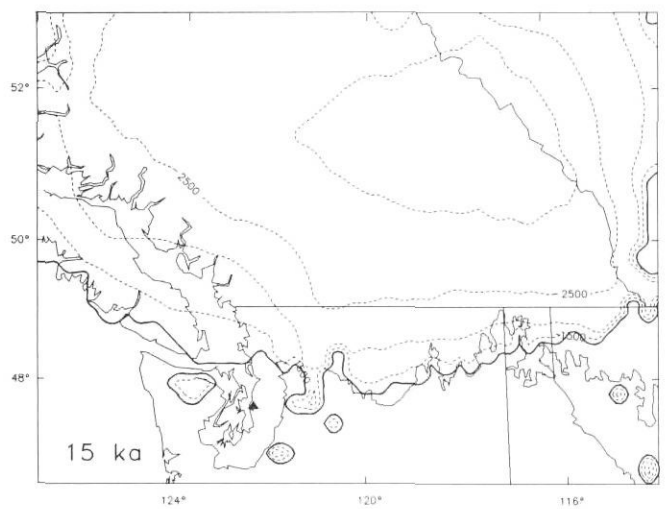

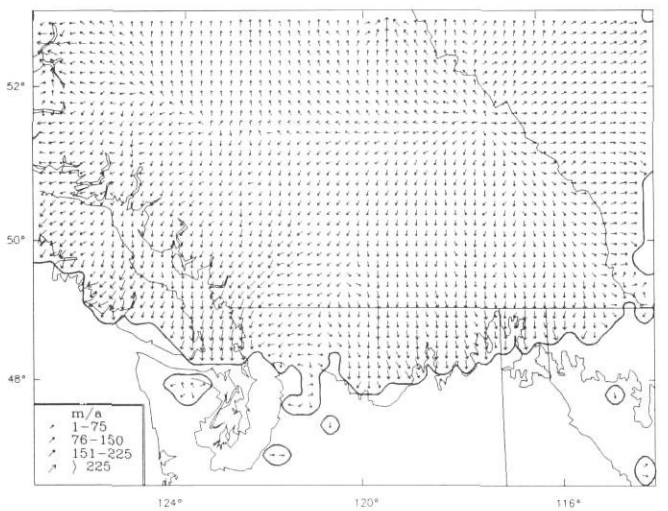

FIGURE 13. Ice configuration at 15 ka.

Configuration des glaces à 15 ka.

17 ka

Ice flow is well integrated, with ice from the Rocky and Coast Mountains merging over the Interior Plateau and being diverted north and south resulting in an ice divide in the north central portion of the study area (Fig. 12). Relatively fast ice streams are flowing into the Georgia Depression from the Coast Mountains and down the Fraser Valley. The ice sheet is quite massive and is steadily advancing southward across interior British Columbia and eastward into the plains of Alberta. One ice-free dated locality is within the ice margin at this time.

15 ka

The ice sheet is near its maximum southern extent. Ice lobes in the central portion of the study area are fairly well developed (Fig. 13). The Puget Lobe is evident but not fully advanced to its Late Wisconsinan maximum margin. The Okanagan Lobe has reached its maximum recorded extent. The ice sheet has developed a central dome over the eastern Interior Plateau and Rocky Mountains. As the ice thickens, the ice flow vectors are less influenced by the underlying topography and more controlled by the ice surface slope. The ice flow vectors now show a radial pattern of ice flow away from the central dome. A dominant ice stream still exists across the Fraser Valley and the southern end of the Georgia Depression.

13 ka

The ice has retreated substantially from its 15 ka configuration (Fig. 14). Ice is rapidly retreating from the Georgia Depression and Vancouver Island is completely deglaciated. The general ice flow pattern has not changed greatly but some minor topographic effects are reappearing along the ice margin. Several dated ice-free localities, all of which are consistent with the ice sheet configuration, are shown.

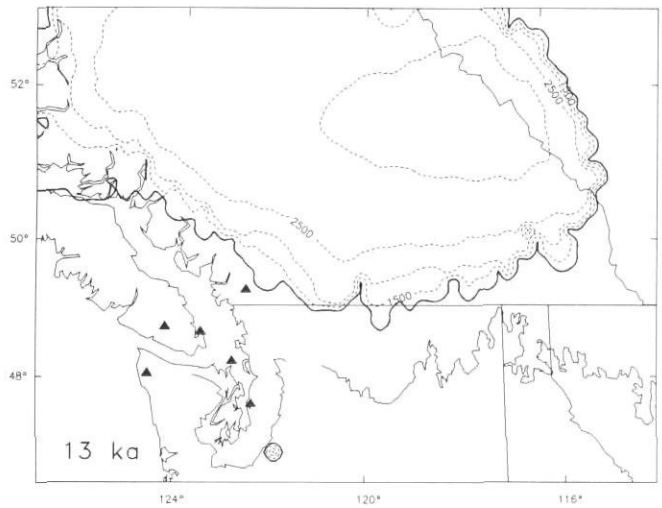

FIGURE 14. Ice configuration at 13 ka.

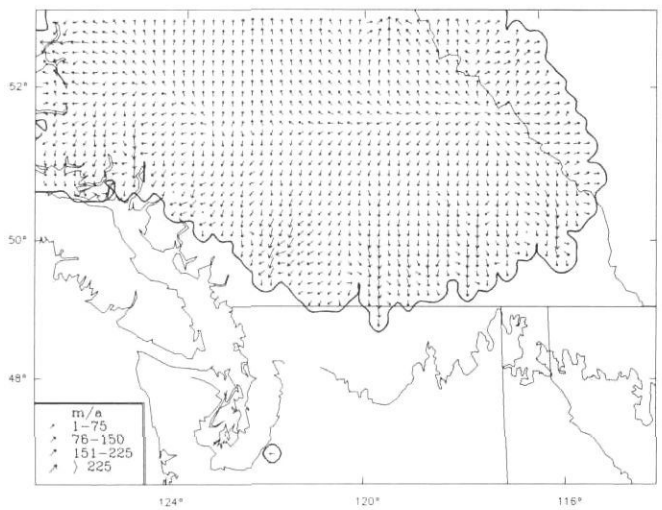

Configuration des glaces à 13 ka.

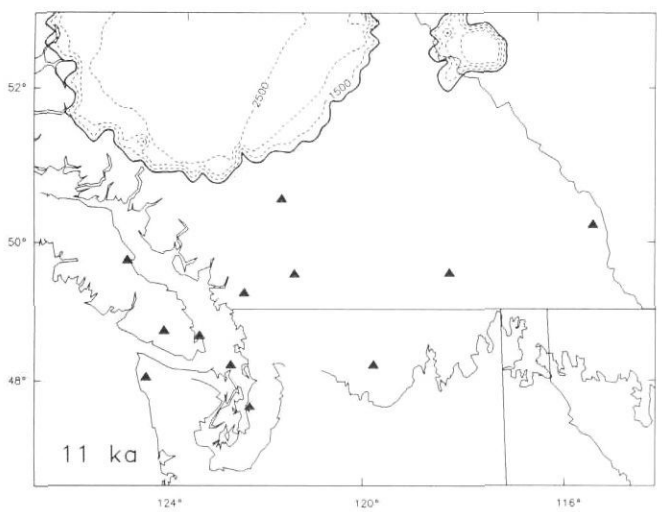

FIGURE 15. Ice configuration at 11 ka.

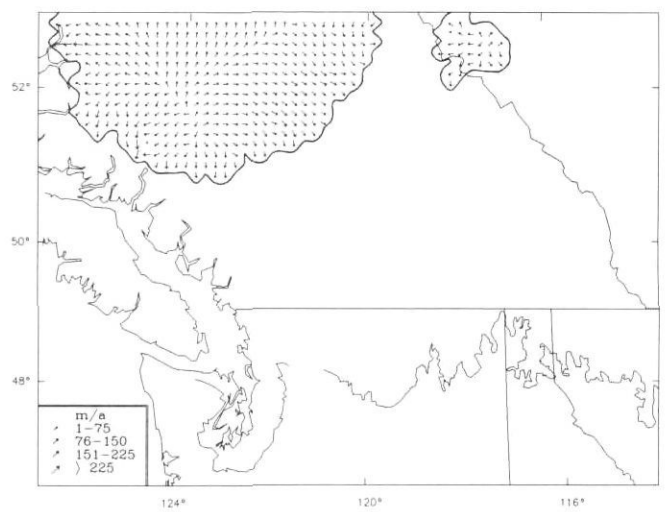

Configuration des glaces à 11 ka.

11 ka

The ice has split into two ice masses — a large Coast Mountain-Interior Plateau ice sheet, and a smaller Rocky Mountain ice cap (Fig. 15). Eastward ice flow off the Coast Mountains forms a sweeping arc starting in a north-east direction and gradually rotating to the south-east. Westward ice flow off the Coast Mountains is being deflected by a small nunatak along the south-west ice margin.

9 ka

All the ice masses are continuing to shrink slowly (Fig. 16). The Coast Mountains ice flow pattern shows a general east-west ice divide corresponding to the axis of the Coast Mountains. Some ice remains on the Interior Plateau. One ice-free location symbol appears near the ice margin in the south-east quadrant of the Coast Mountains ice cap. The significance of this point is uncertain. The dated location is near the modern terminus of the Tiedemann Glacier (Clague, 1980, 1981). This location would also plot within the model's modern ice margin used at the start of the simulation.

GENERAL OBSERVATIONS

Based on the relationship between the ice margin and radiocarbon dated localities, the chronology of ice growth and decay presented by this modeling experiment appears reasonable. With only minor exceptions, the timing of advance and retreat is consistent with the limits placed by radiocarbon date information.

The maximum areal extent of the ice sheet occurs between 15 and 14 ka; the central section of the southern margin follows the Late Wisconsinan margin fairly well at this time. The Puget Lobe of western Washington does not reach the recorded Late Wisconsinan maximum position. The most probable explanation for this is the exclusion of a basal sliding function. Booth (1986) reports that basal sliding was an extremely important process for mass flux in the Puget Lobe. The exclusion of basal sliding from the model may explain the limited extent of the Puget Lobe in the simulation results.

The model ice front is also under-advanced at the eastern end of the southern margin. This may be a boundary effect.

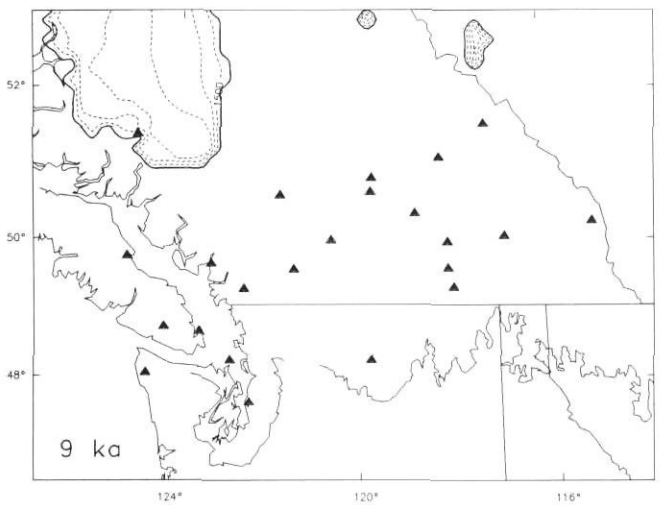

FIGURE 16. Ice configuration at 9 ka.

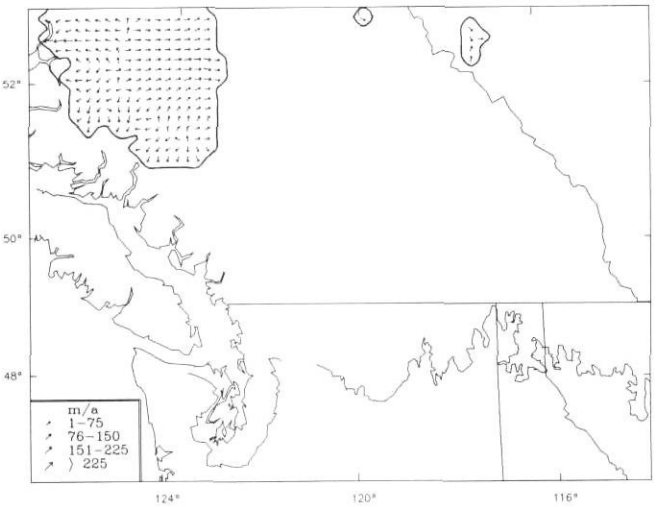

Configuration des glaces à 9 ka.

Locke and Semerad (1988) have theorized that the Flathead Lobe, the most eastern lobe of the southern margin, was primarily fed by local alpine glaciers. The source for these local glaciers would be located just east of the study area. Apparently the exclusion of high elevation areas to the east of the modeling grid limits ice growth in the eastern portion of the solution region.

Although the position of the eastern margin of the Cordilleran Ice Sheet in Alberta is problematic (Rutter, 1984), based on the ice extent shown by Clague (1989) (Fig. 17, this paper) it appears the model over-advances to the east. This may stem from the net mass balance rates used in the model, the use of a constant ELA drop throughout the study area, or boundary condition problems.

Ice surface elevations from the model agree well with geologic evidence along the outer portions of the ice sheet (Fig. 17). However, a possible discrepancy exists near the center of the model ice sheet where a high elevation (above 3000 m) region exists. The ice thickness is too great in this region. This may indicate the need for further refinement in the flow law parameters used in the model.

The ice flow vectors generated by the model are calculated from the x and y ice flux components. The ice flux is computed from ice thickness and ice surface slope. The vectors represent the average ice flow direction in the ice column. This limits the validity of comparison against geologic ice flow indicators which record basal flow directions; however, some general observations can be made.

During the ice advance phase of the simulation, the ice flow vectors and the general location of the north-south ice divide agree well with recorded ice flow directions (Fig. 17). As the ice sheet reaches its maximum extent, a high elevation dome over the eastern portion of the study area shifts the ice flow vectors over the Interior Plateau from a south-easterly to a south-westerly direction. This pattern continues through deglaciation until enough ablation has occurred to remove the influence of the ice dome. In general, the ice flow vectors predicted

FIGURE 17. Extent, flow directions and maximum surface elevations (m) of the Late Wisconsinan Cordilleran Ice Sheet within the study area (after Clague, 1989). Maximum surface elevations are based on modern sea level and are uncorrected for isostatic depression. Margin of ice sheet dashed where location is approximate.

Étendue, directions de l'écoulement et altitudes maximales des surfaces englacées (m) de l'Inlandsis de la Cordillère du Wisconsinien supérieur à l'intérieur de la région à l'étude (d'après Clague, 1989). Les altitudes maximales des surfaces sont fondées sur le niveau de la mer actuel et ne tiennent pas compte de l'abaissement isostatique. Les limites glaciaires incertaines sont en tireté.

by the model agree with the glacial geology when ice flow is not dominated by this ice dome.

The amount of ELA rise during deglaciation is difficult to specify. Deglaciation studies suggest that the ELA rose to a level above much of the ice surface during ice retreat (Fulton, 1967). In the simulation results presented here, an increase in ELA to 400 m above modern was required to obtain a nearly complete deglaciation of the study area.

The high ELA required for deglaciation is likely linked to assumptions made during formulation of the model. The exclu-

sion of basal sliding, ablation through calving, and isostatic compensation may be of particular importance. Basal sliding was a very important process for mass flux in the Puget Lobe (Booth, 1986). Its exclusion from the model may have eliminated a process which may have allowed a more rapid deglaciation at a relatively lower ELA. Increased ablation through calving may also have increased the rate of deglaciation for the Puget Lobe by providing an additional mechanism for removing mass from the ice sheet. Addition of this process to the model may allow for rapid deglaciation without an ELA far above modern.

The relatively high deglaciation ELA may also be linked to the exclusion of isostatic compensation from the model. Crustal depression caused by the ice would lower the surface elevation of the ice sheet, effectively raising the relative ELA. This effect may be represented in the simulation results by the higher than modern ELA required for rapid deglaciation. Points along the British Columbia coastline experienced isostatic depression on the order of 250 m during the Late Wisconsinan Glaciation (Clague, 1983). Although only a portion of the 400 m rise used in the model, it demonstrates the magnitude of depression which would be expected if isostatic compensation were included.

SUMMARY

The model simulates the growth and decay chronology of the Late Wisconsinan Cordilleran Ice Sheet well. The character of ice growth and decay generally matches what has been deduced from the geologic record. Although testing the ice flow directions is problematic, the general trends are consistent with the geologic evidence. Deviations from recorded ice flow directions occur when a high elevation ice dome develops in the central portion of the study area.

Considering the grid spacing used, the central portion of the southern ice margin agrees well with the maximum Late Wisconsinan margin. The limited size of the Puget Lobe in the simulation results is likely due to the exclusion of basal sliding. The restricted extent of ice along the eastern end of the southern margin suggests accumulation regions east of the study area may have been an important source of ice for this region. Along the eastern ice margin in Alberta, the model advances the ice margin too far eastward. Various factors such as net mass balance rates or boundary conditions may be responsible for this situation.

While ice surface elevations along the outer portions of the ice sheet are reasonable, the high elevations near the center of the ice do not agree with the geologic evidence. This inconsistency should be addressable through adjustment of the ice flow law parameters or the addition of an isostatic compensation function.

Although it does not necessarily represent a unique solution, the ELA history curve used in this study does conform with postulated ELA decreases and variations in solar radiation, while providing an ice sheet reconstruction chronology consistent with the geologic evidence. The model's response to different paleoclimatic scenarios can easily be investigated by modifying the ELA history curve.

The results from this study indicate that the computer model developed here is capable of simulating the history of the last Cordilleran Ice Sheet in a manner consistent with a majority of the geologic evidence. The reconstructions from this model provide insights into the dynamics of the ice sheet not recorded in the glacial geology.

ACKNOWLEDGEMENTS

I sincerely appreciate the editorial comments of R. Craig and J. Stamm and thank them for their assistance throughout this project.

This research was performed under appointment to the Nuclear Engineering, Health Physics, and Radioactive Waste Management Fellowships program administered by Oak Ridge Associated Universities for the U.S. Department of Energy. Access to supercomputing facilities was provided through a grant from the Ohio Supercomputer Center. I also thank C. F. Raymond, D. Fisher and an anonymous reviewer for their useful comments.

REFERENCES

Alley, N. F., 1979. Middle Wisconsin stratigraphy and climatic reconstruction, southern Vancouver Island, British Columbia. Quaternary Research, 11: 213-237.

Andrews, J. T. and Mahaffy M. A. W., 1976. Growth rate of the Laurentide Ice Sheet and sea level lowering (with emphasis on the 115,000 B.P. sea level low). Quaternary Research, 6: 167-183.

Booth, D. B., 1986. Mass balance and sliding velocity of the Puget Lobe of the Cordilleran Ice Sheet during the last glaciation. Quaternary Research, 25: 269-280.

——— 1987. Timing and processes of deglaciation along the southern margin of the Cordilleran Ice Sheet, p. 71-90. *In* W. F. Ruddiman and H. E. Wright Jr., eds., North America and Adjacent Oceans During the Last Deglaciation. The Geology of North America, K-3, Geological Society of America, Boulder, Colorado, 509 p.

Budd, W. F. and Smith, I. N., 1981. The growth and retreat of ice sheets in response to orbital radiation changes, p. 369-409. *In* I. Allison, ed., Sea Level Ice and Climatic Change. International Association of Hydrological Sciences: 131.

——— 1987. Conditions for growth and retreat of the Laurentide Ice Sheet. Géographie Physique et Quaternaire, 41: 279-290.

COHMAP Members, 1988. Climatic change of the last 18,000 years: observations and model simulations. Science, 241: 1043-1052.

Clague, J. J., 1975. Glacier-flow patterns and the origin of Late Wisconsinan till in the southern Rocky Mountain Trench, British Columbia. Geological Society of America Bulletin, 86: 721-731.

——— 1980. Late Quaternary geology and geochronology of British Columbia, part 1: radiocarbon dates. Geological Survey of Canada, Paper 80-12, 28 p.

——— 1981. Late Quaternary geology and geochronology of British Columbia, part 2: summary and discussion of radiocarbon-dated Quaternary history. Geological Survey of Canada, Paper 80-35, 41 p.

——— 1983. Glacio-isostatic effects of the Cordilleran Ice Sheet, British Columbia, p. 321-343. *In* D. E. Smith and A. G. Dawson, eds., Shorelines and Isostasy. Academic Press, London, 387 p.

——— 1989. Cordilleran Ice Sheet, p. 40-42. *In* R. J. Fulton, ed., Chapter 1 of Quaternary Geology of Canada and Greenland. The Geology of North America, K-1, Geological Society of America, Boulder, Colorado, 839 p.

Clague, J. J., Saunders, I. R. and Roberts, M. C., 1988. Ice-free conditions in southwestern British Columbia at 16,000 years B.P. Canadian Journal of Earth Sciences, 25: 938-941.

Denton, G. H. and Hughes, T. J., 1981. The Last Great Ice Sheets. Wiley Interscience, New York, 484 p.

Easterbrook, D. J., 1986. Stratigraphy and chronology of Quaternary deposits of the Puget Lowland and Olympic Mountains of Washington and the Cascade Mountains of Washington and Oregon, p. 145-159. *In* V. Sibrava, D. Q. Bowen and G. M. Richmond, eds., Quaternary Glaciations in the Northern Hemisphere. Pergamon Press, New York, 514 p.

Fulton, R. J., 1967. Deglaciation studies in Kamloops region, an area of moderate relief, British Columbia. Geological Survey of Canada, Bulletin 154, 36 p.

——— 1984. Quaternary glaciation, Canadian Cordillera, p. 39-48. *In* R. J. Fulton, ed., Quaternary Stratigraphy of Canada — A Canadian Contribution to IGCP Project 24. Geological Survey of Canada, Paper 84-10, 210 p.

Haeberli, W., 1985. Fluctuations of glaciers 1975-1980 (vol. IV). International Commission on Snow and Ice of the International Association of Hydrologic Sciences and United Nations Education, Science and Culture Organization, Paris, 256 p.

Haeberli, W. and Muller, P., 1988. Fluctuations of glaciers 1980-1985 (vol. V). International Association of Hydrologic Sciences/United Nations Environmental Program/United Nations Education Science and Culture Organization, World Glacier Monitoring Service, Zurich, 289 p.

Heusser, C. J., 1973. Environmental sequence following the Fraser advance of the Juan de Fuca Lobe, Washington. Quaternary Research, 3: 284-306.

Heusser, C. J., Heusser, L. E. and Streeter, S. S., 1980. Quaternary temperatures and precipitation for the north-west coast of North America. Nature, 286: 702-704.

Hughes, T. J., 1985. The great Cenozoic Ice Sheet. Palaeogeography, Palaeoclimatology, Palaeoecology, 50: 9-43.

Hughes, T., 1987. Ice dynamics and deglaciation models when ice sheets collapsed, p. 183-220. *In* W. F. Ruddiman and H. E. Wright Jr., eds., North America and Adjacent Oceans During the Last Deglaciation. The Geology of North America, K-3, Geological Society of America, Boulder, Colorado, 509 p.

Locke, W. W. and Semerad, E., 1988. A testable hypothesis regarding Late-Pleistocene ice-cap glaciation of the northern Rocky Mountains of Montana. Geological Society of America Abstracts with Programs, 20: 428.

Mahaffy, M. A. W., 1974. A three-dimensional numerical method for computing the load distribution of ice sheets with time. M.S. thesis, University of Colorado, 74 p.

——— 1976. A three-dimensional numerical model of ice sheets: tests on the Barnes Ice Cap, Northwest Territories. Journal of Geophysical Research, 81: 1059-1066.

Mehringer, P. J. Jr., Sheppard, J. C. and Foit, F. F. Jr., 1984. The age of Glacier Peak tephra in west-central Montana. Quaternary Research, 21: 36-41.

Meier, M. F., Tangborn, W. V., Mayo, L. R. and Post, A., 1971. Combined ice and water balances of Gulkana and Wolverine Glaciers, Washington, 1965 and 1966 hydrologic years. U.S. Geological Survey Professional Paper 715-A, 23 p.

Mullineaux, D. R., Waldron, H. H. and Rubin, M., 1965. Stratigraphy and chronology of late interglacial and early Vashon glacial time in the Seattle area, Washington. U.S. Geological Survey Bulletin 1194-0, 10 p.

Oerlemans, J., 1981. Modeling of Pleistocene European ice sheets: some experiments with simple mass-balance parameterizations. Quaternary Research, 15: 77-85.

Porter, S. C., 1977. Present and past glaciation threshold in the Cascade Range, Washington, U.S.A.: topographic and climatic controls, and paleoclimatic implications. Journal of Glaciology, 18: 101-116.

——— 1978. Glacier Peak tephra in the North Cascade Range, Washington: stratigraphy, distribution, and relationship to late-glacial events. Quaternary Research, 10: 30-41.

Porter, S. C., Pierce, K. L. and Hamilton, T. D., 1983. Late Wisconsin mountain glaciation in the western United States, p. 71-111. *In* H. E. Wright Jr., ed., Late-Quaternary Environments of the United States, vol. 1. University of Minnesota Press, Minneapolis.

Prest, V. K., Grant, D. R. and Rampton, V. N., 1968. Glacial map of Canada. Geological Survey of Canada, Map 1253A.

Radok, U., Barry, R. G., Jenssen, R. A., Kiladis, G. N. and McInnes, B., 1982. Climatic and physical characteristics of the Greenland Ice Sheet, parts I and II. Cooperative Institute for Research in Environmental Sciences, University of Colorado, Boulder, 193 p.

Roberts, B. L., 1990. A computer model of the Late Wisconsinan Cordilleran Ice Sheet. Ph.D. dissertation, Kent State University, 288 p.

Rutter, N. W., 1984. Pleistocene history of the western Canadian ice-free corridor, p. 50-56. *In* R. J. Fulton, ed., Quaternary Stratigraphy of Canada — A Canadian Contribution ot IGCP Project 24. Geological Survey of Canada, Paper 84-10, 210 p.